

E9039
5/18/95

NASA Technical Memorandum 106685

Comparison of Numerical Results and Multicavity Purge and Rim Seal Data With Extensions to Dynamics

Mahesh M. Athavale and Andrzej J. Przekwas
CFD Research Inc.
Huntsville, Alabama

and

Robert C. Hendricks and Bruce M. Steinmetz
Lewis Research Center
Cleveland, Ohio

Prepared for the
Third Northern Ohio Technical Symposium "Aerospace Today"
sponsored by the American Institute of Aeronautics and Astronautics
Cleveland, Ohio, May 16, 1994



National Aeronautics and
Space Administration

COMPARISON OF NUMERICAL RESULTS AND MULTICAVITY PURGE AND RIM SEAL DATA WITH EXTENSIONS TO DYNAMICS

Mahesh M. Athavale and Andrzej J. Przekwas
CFD Research Inc.
Huntsville, AL 35805

Robert C. Hendricks and Bruce M. Steinmetz
NASA Lewis Research Center
Cleveland, OH 44135

SUMMARY

The computation of flows within interconnected, multiple-disk cavities shows strong interaction between the cavities and the power stream. For this reason, simulations of single cavities in such cases are not realistic; the complete, linked configuration must be considered.

Unsteady flow fields affect engine stability and can engender power-stream-driven secondary flows that produce local hot spotting or general cavity heating. Further, a concentric whirling rotor produces a circumferential pressure wave, but a statically eccentric whirling rotor produces a radial wave; both waves affect cavity ingestion and the stability of the entire engine. It is strongly suggested that seals be used to enhance turbojet engine stability. Simple devices, such as swirl brakes, honeycomb inserts, and new seal configurations, should be considered.

The cost effectiveness of the NASA Lewis Research Center seals program can be expressed in terms of program goals (e.g., the Integrated High-Pressure/Temperature Engine Technology (IHPTET) cannot be achieved without such a program), cost (savings to \$250 million/1-percent decrease in specific fuel consumption), and indirect benefits (reduction of atmospheric NO_x and CO₂ and reduction of powerplant downtime).

INTRODUCTION

The ingestion of power-stream fluids into disk cavities can engender thermal hot spots, hub and lubricant overheating, undesirable leakage into the lubricant systems, erratic rubbing, disk warpage, and reduced bearing life. Single-cavity flow experiments and computations are insufficient to assess the effects of ingestion in a multiple-cavity turbojet or turbo-machine configuration.

Single-cavity testing, however, is instructive and represents a major challenge in experimental facility design and analytical and/or numerical evaluation as well as in instrumentation and data evaluation. Four jet engine rim seal configurations connected to a single fixed-geometry cavity configuration were experimentally evaluated by Gruber, Daniels, and Johnson (1987). The numerical codes CFDACE and SCISEAL were used to calculate the interactive coupling of the power stream, the secondary cavity flow, and the seal. The cooling effectiveness parameter ϕ was calculated for selected values of the dimensionless purge flow and compared with the data. At low purge flows, the results agreed within 18 percent and at higher purge flows, within 2 percent as illustrated in table I. The details are presented by Athavale et al. (1994). INDSEAL, a collection of seal codes, is described by Shapiro (1994).

Presented herein are the results of combined-cavity, purge, and power-stream flow solutions for a simulation of a blocked interstage flow geometry similar to, the experimental rig of Daniels and Johnson (1993). Comparisons are made of CO₂ purge flow contours with temperature (the thermal management problem). Also presented are discussions of the effects of unsteady flows and machine dynamics. While the blocked flow does not represent interstage geometry, the results do demonstrate coupled-flow computations.

MULTIPLE-CAVITY RESULTS

Multiple-cavity testing was carried out in a companion apparatus by Daniels and Johnson (1993) in a configuration simulating the Space Shuttle Main Engine (SSME) high-pressure fuel turbopump (HPFTP). In the simulation the HPFTP blade/rotor configuration was replaced by a series of flow blocks to assess the CO₂ distribution within the cavities. The upper portion of figure 1(a) represents the HPFTP geometry; the lower portion of the figure represents the simulated

HPFTP cavities. The actual test configuration then becomes that illustrated in figure 1(b). The grid for the composite geometry is illustrated in figure 1(c) for the right half of the simulated HPFTP configuration. This geometry represents a solid interstage stem configuration with leakage through the labyrinth seal to the aft cavity. The actual geometry permits leakage through the interstage stem to the aft cavity. This leakage was unknown and not simulated. The computational results presented herein represent a two-dimensional simulation.

The mixture fraction contours within the multiple connected cavities (grid shown in fig. 1(c)) for purge flows F1 and F2 interacting with the power stream F3 are illustrated for three purge flow rates $\eta_t = 0.005, 0.010$, and 0.025 in figure 2. The contours represent the dilution of the purge flow CO_2 (red representing the undiluted state).

At a low purge flow rate, $\eta_t = 0.005$, the purge flows are rapidly diluted (fig. 2(a)). For example, only a small portion of the purge flow F1 (or F2) reaches region V, representing poor purging and fluid ingestion. The power-stream flow F3 is ingested into all the cavities.

At an intermediate purge flow rate, $\eta_t = 0.010$, the purge flows F1 and F2 are less diluted, and less power-stream ingestion F3 is noted, especially in the forward cavity and region II (fig. 2(b)).

At a high purge flow rate, $\eta_t = 0.025$, the purge flows F1 and F2 are virtually undiluted with little or no power-stream ingestion into the cavities (fig. 2(c)). The interesting feature is that both the F1 and F2 purges are effective in above-the-blade-platform cooling (i.e., purge flow is dumped into the power stream). Dilution of the power steam is small with the interfaces between purge flow and power-stream flow clearly defined.

The streamline contours for regions representing the power stream, the rim seal region, and region V (the cavity connection region for cooling beneath the blade platform) are shown in figure 3. Combining the information of figures 2 and 3 indicates that at a low purge flow rate, $\eta_t = 0.005$, circulation of ingested fluid occurs, but that at a high purge flow rate, $\eta_t = 0.025$, little ingestion is noted.

To clarify the effects of the circulation of ingested fluid, first, note that the computations are two-dimensional simulations of the apparatus for a solid interstage stem by Daniels and Johnson (1993) and that the opening under the blade platform is a two-dimensional representation of several feed slots in the rotor disk along the circumference and flows to the aft cavity are restricted by the solid interstage stem. Second, note the stepdown region in the downstream part of the blade simulation (see fig. 1 for geometry). Third, note that it is difficult to penetrate the boundary layer of a rotating disk and that the rotating feed holes under the blade platforms, with attendant recirculation zones of their own, would be even more difficult to penetrate.

With these limitations in mind, note the streamlines in the upstream rim seal (fig. 3(d)) for $\eta_t = 0.002$. A vortex zone appears, but the power streamlines do not penetrate the cavity. At the downstream rim seal (fig. 3(e)), the power stream recirculates to the forward cavity and out the upstream rim seal. For this geometry and the boundary conditions of equal pressure, power-stream ingestion is in the form of a circulation around the blade platform. Increasing the purge flows to $\eta_t = 0.01$ enhances both the vortex zone and the recirculation about the blade platform (figs. 3(f) and (g)).

The interactive effects of multiple-cavity purge flows with the power stream are significant but are undetermined from computations that isolate individual cavity power-stream interactions (computations based on one cavity will be incorrect). Further, the actual geometry has several holes in the interstage stem that permit large flows into the aft cavity. These multiply connected multicavity flows are currently under investigation (see fig. 3(h)).

THERMAL MANAGEMENT SIMULATION

At low rotational speeds, replacing the scalar mass equations for the calculation of CO_2 distributions with the scalar energy equation (without $\tau:u$ (tensor product of stress and velocity)) provides a mapping of the thermal contours similar to those of CO_2 . Thus, once the thermal scaling parameter is established, the CO_2 profiles are equivalenced to the thermal profiles.

For an inlet axial velocity of 400 m/s and a tangential velocity of 70 m/s, an inlet pressure P_{inlet} and temperature T_{inlet} of 860 kPa and 1200 K, respectively, purge pressure and temperature of 690 kPa = $0.8 P_{\text{inlet}}$ and 700 K, respectively, and cavity purge flow $\eta_t = 0.001$, the cooling effectiveness is 0.77 for United Technology Research Corporation (UTRC) cavity configuration 1 (Graber, Daniels, and Johnson, 1987) and 0.53 for the UTRC data of Gruber, Daniels, and Johnson (1987) at lower pressure and velocities. The CO_2 concentration contours (fig. 4(a)) show large gradients near the rim seal. Corresponding temperature solutions are of similar form even when viscous dissipation is included ($\tau:u$) (fig. 4(b)). Comparing figures 4(a) and (b) shows similar gradients when all other parameters are held constant.

Increasing the purge flow to $\eta_t = 0.008$ increases the cooling effectiveness to 0.9999 with F1 contours (CO_2 concentration) as illustrated in figure 4(c). The CO_2 gradients are strongest in the rim seal with a nearly 1:1 correspondence with temperature (fig. 4(d)).

At high rotational speeds, the temperature contours can be expected to be different because the dissipation is a significant part of the power required for rotation and is released in the form of cavity heating. In a discussion of compressor discharge face seal experimental work reported by Munson (1993), most of the cavity heat was generated from viscous dissipation (windage losses).

UNSTEADY FLOW AND DYNAMICS

Athavale, Przekwas, and Hendricks (1993a) illustrated the use of injected vortices to control blade/vane-generated vortical flows engendered by simulated tip seal configurations. The up-to-30-percent vortical flows in simulated blade passages could be reduced to smaller vortical flows with enhanced throughflow.

Athavale, Przekwas, and Hendricks (1993b) showed the simulated effects of a displaced rotor on the ingestion and suction of flows in a rotor cavity. Such rotor displacements can produce circumferential flows within the cavity, causing hot spots which are phased with the rotor or culminate at nodal points that may be irregular. The effects of nonuniform power-stream ingestion can be severe. Such cavity flow ingestion has been noted in the nozzle/powerhead interface for the SSME, where seal degradation leads to overheating and warpage of the mating flange (Hendricks et al., 1992).

Unsteady flow fields affect rotor stability. If the rotor is within its critical range, the effects can be catastrophic. Generally, the rotor is perturbed and dampers are employed to prevent large shaft excursions. To illustrate the differences between a rotor whirling about a position centered within the housing and one with static eccentricity, a simulated shaft seal configuration was analyzed by using the code SCISEAL. When the static eccentricity is zero and the whirl speed is twice the rotor speed, the pressure field leads the rotor by nearly 70° (fig. 5(a)). As a rule, the angle changes with whirl speed (for supersynchronous whirl the lead angle > 0 , and for subsynchronous whirl the lead angle < 0 ; i.e., the maximum pressure will lag the rotor). Further, the magnitude is unchanged with circumferential position; it appears as a circumferential wave rolling about the seal clearance. Contrast these results with those of figure 5(b), where the static eccentricity is 0.7. The whirling rotor produces a pressure that still leads the rotor in a reciprocating-pistonlike manner. The magnitude of the pressure at any fixed point on the housing is cyclic, like a radial oscillation. The implication for interactions between secondary and power-stream flows is that rotating or radial oscillations can be produced. The ellipticity of the rim interface and static eccentric whirl of the shaft cause local starvation of the coolant flow with fractions of the power stream fed directly into the cavities. Local hot spotting and abnormal disk-cavity heating ensue. Such nonuniformities lead to a reduction in disk life and disk bowing which tends to "wipe out" the inner and outer gas path seals, only exacerbating the problem.

STABILIZATION OF TURBOMACHINES BY SEALS

Over the flight operations envelope, turbojet rotor clearances can change from, for example, 10 to 50 mils. Even under these circumstances, seal rub-in of the housing and dampers must be employed to maintain rotor stability. With a goal to reduce engine clearances and decrease specific fuel consumption (SFC) come new problems in flow and rotor stability.

The seals can play a major role in stabilizing components of the turbojet engine, just as the seals stabilized the SSME turbomachines permitting the space shuttle to be operational. Simple devices, such as swirl brakes upstream of labyrinth seals, honeycomb inserts, and new seals such as brush, finger, damper, and labyrinth/brush combinations, all enhance turbomachine stability.

It is strongly suggested that seal stabilization of the turbomachine be pursued as a line item.

COST EFFECTIVENESS

The NASA Lewis Research Center seals program, including codes SCISEAL and INDSEAL, is intended for aeronautics, space/rocket engines, and industrial programs. Its focus is on the interactive dynamics and thermal management of seals, cavities, and power-stream elements, both below and above the blade platform. The goals of Advanced Subsonic Technologies (AST), High-Speed Research (HSR), and Integrated High-Pressure/Temperature Engine Technology (IHPTET) programs cannot be met without a seals program and neither can the goals established by the NASA Marshall Space Flight Center for turbomachines. (The IHPTET goals, in terms of increments and aircraft fuel/operations costs, are presented in tables II and III).

Comparative engine testing (T-700) of a compressor discharge dual-brush seal and an advanced labyrinth seal provided these proven results (Hendricks et al., 1994):

- (1) SFC gain was greater than 1 percent.
- (2) Compressor discharge pressure (CDP) seal leakage control affected the entire engine.

For a 10-lb/s-class engine with 0.1-percent CDP seal leakage, the SFC gain was not from changing the CDP seal alone because the power-stream flow in the compressor changed and the discharge pressure increased (presumably combustor and turbine flows also changed).

The potential SFC gains to 4 percent for regional class engines and to 3 percent for large engines would alone produce an annual fuel savings of up to \$1 billion (based on U.S. fuel savings of \$250 million per year for a 1-percent SFC gain (M. Stibich and E.R. Mayhew, 1994, WL/PTOF, Wright Patterson Air Force Base, Dayton, Ohio, private communication). An indirect and more important benefit is environmental: NO_x and CO₂ decrease directly with a decrease in fuel consumption; also helped would be the conservation of natural resources. Industrial spinoffs include electric power generation, where electric powerplant downtime costs \$1 million per day, and airline engine changeouts, which cost \$1 million per engine.

CONCLUSIONS

Presented herein are the results of combined-cavity, purge, and power-stream flow solutions for the simulated SSME high-pressure fuel turbopump (HPFTP) experimental data of W.A. Daniels and B.V. Johnson (Experimental Investigation of Turbine Disk Cavity Aerodynamics and Heat Transfer, NASA CR-193831, 1993) and discussions of the effects of unsteady flows and machine dynamics.

1. The interactions of the multiple-cavity purge flows with the power stream are significant. Computations based on one cavity are simply incorrect. The results do not match the experimental data. Further computations are necessary to assess the effect of rotating boundary layers on secondary flow ingestion.
2. A thermal management simulation using CO₂-air mixtures provides flow distribution details at low rotational speeds, but at high rotational speeds the relation to temperature is clouded by cavity dissipation, which can represent most of the cavity heat generation.
3. Unsteady flow and turbomachine dynamics can engender power-stream-driven secondary flows that produce local hot spotting or general cavity heating. Brush seals can be effective in mitigating circumferential maldistribution of energy.
4. Unsteady flow fields affect engine stability. A rotor whirling about a position centered within the housing produces a circumferential pressure wave; a statically eccentric whirling rotor produces a radial wave. Both waves affect cavity ingestion and the stability of the entire engine and must be absorbed by dampers.
5. It is strongly suggested that seals be used to enhance turbojet engine stability and reduce the large range of required operational clearances. Simple devices, such as swirl brakes, honeycomb inserts, and new seals such as brush, finger, damper, and labyrinth/brush combinations, all enhance turbomachine stability.
6. The cost effectiveness of the NASA Lewis Research Center seals program (codes SCISEAL and INDSEAL and experiments) centers on program goals, cost, and indirect benefits. The goals of Lewis' Advanced Subsonic Technologies, High-Speed Research, and Integrated High-Pressure/Temperature Engine Technology programs and those of other NASA centers require such a program. The potential annual saving in fuel costs alone is up to \$1 billion (U.S. fuel saving of \$250 million per year for a 1-percent gain in specific fuel consumption). Environmental cleanup benefits indirectly because NO_x and CO₂ decrease directly with a decrease in fuel consumption. Industrial spinoffs include reducing powerplant downtime costs of \$1 million per day and airline engine changeout costs of \$1 million per engine.

REFERENCES

Athavale, M.M.; Przekwas, A.J.; and Hendricks, R.C.: Driven Cavity Simulation of Turbomachine Blade Flows with Vortex Control. AIAA Paper 93-0390, 1993a.

Athavale, M.M.; Przekwas, A.J.; and Hendricks, R.C.: A Numerical Study of the Flow Field in Enclosed Turbine Disk Cavities in Gas Turbine Engines. ISROMAC-4, 4th International Symposium on Transport Phenomena and Dynamics of Rotating Machinery, Hemisphere Pub. Corp., Washington, DC, 1993b, pp. 122-131.

Athavale, M.M. et al.: SCISEAL—A Three-Dimensional CFD Code for Accurate Analyses of Fluid Flow and Forces in Seals. Presented at the 1994 Conference on Advanced Earth-to-Orbit Propulsion Technology, NASA Marshall Space Flight Center, Huntsville, AL, May 1994.

Daniels, W.A.; and Johnson, B.V.: Experimental Investigation of Turbine Disk Cavity Aerodynamics and Heat Transfer. (UTRC-93-957878-27, United Technologies Research Center, NASA Contract NAS8-37462) NASA CR-193831, 1993.

Graber, D.J.; Daniels, W.A.; and Johnson, B.V.: Disk Pumping Test. Report AFWAL-TR-87-2050, Pratt and Whitney Aircraft, West Palm Beach, FL, 1987.

Hendricks, R.C. et al.: Static Brush Seals for Propulsion System Interfaces. Advanced Earth-To-Orbit Propulsion Technology 1992, vol. 1, R.J. Richmond and S.T. Wu, eds., NASA CP-3174-Vol-1, 1992, pp. 432, 439.

Hendricks, R.C. et al.: Relative Performance Comparison Between Baseline Labyrinth and Dual-Brush Compressor Discharge Seals in a T-700 Engine Test. To be published as NASA TM-106360, 1994.

Munson, J.H.: Testing of a High Performance Compressor Discharge Seal. AIAA Paper 93-1997, 1993.

Shapiro, W.: Industrial Code for Seal Analysis. Presented at the 1994 Conference on Advanced Earth-to-Orbit Propulsion Technology, NASA Marshall Space Flight Center, Huntsville, AL, May 1994.

Uchida, T.; and Mizuno, H.: Next-Generation SST: Technology Requirements. Aerospace Eng., vol. 14, no. 4, 1994, pp. 29-31.

TABLE I—COMPUTATIONS VERSUS EXPERIMENTS

[Cooling effectiveness parameter, φ^a ; $Re_j = 5.0 \times 10^6$, $V_{\varphi j} \equiv R_0 \Omega$.]

Configuration	Dimensionless coolant flow parameter, η_t	Cooling effectiveness parameter, φ		Deviation, percent
		Experimental ^b	Calculated	
1	0.001	0.53	0.63	19
	.002	.77	.802	4
	.004	.94	.972	3
	.008	1	.997	-0.3
2	0.001	0.89	0.95	7
	.008		.99	—
3	0.001	0.57	0.611	7
	.008	.98	.99	1
4	0.001	0.5	0.589	18
	.008	.98	.965	-2

^aNumerical results computed using assumed main-flow conditions with axial velocity ranging from 120 to 150 m/s.

^bExperimental data from Graber, Daniels, and Johnson (1987).

TABLE II.—INTEGRATED HIGH-PRESSURE/TEMPERATURE
ENGINE TECHNOLOGY PROGRAM GOALS^a

Turbofan/turbojet	
Thrust/weight, percent	100
Turbine inlet temperature, T_{41} , °C (°F)	500 (900)
Fuel burn, percent	-40
Compressor outlet temperature, T_3 , °C (°F)	222 (400)
Compressor	
Efficiency, percent	5
Weight, percent	-50
Stage loading, percent	50
Compressor outlet temperature, T_3 , °C (°F)	222 (400)
Leakage, percent	-60
Turboshaft/turboprop	
Specific fuel consumption, percent	-40
Power/weight, percent	120
Turbine inlet temperature, T_{41} , °C (°F)	556 (1000)
Compressor	
Pressure ratio	40
Number of stages	2
Efficiency, percent	3
Expendable engines	
Thrust/airflow, percent	100
Specific fuel consumption, percent	-40
Cost, percent	-60
Turbine inlet temperature, T_{41} , °C (°F)	778 (1400)
Compressor outlet temperature, T_3 , °C (°F)	778 (1400)
Compressor	
Efficiency, percent	2
Compressor outlet temperature, T_3 , °C (°F)	778 (1400)

^aBased on information from M. Stibich and E.R. Mayhew, 1994,
WL/POTF, Wright Patterson Air Force Base, Dayton, Ohio.

TABLE III.—AIRCRAFT FUEL CONSUMPTION
AND OPERATIONAL COSTS^a

U.S. fuel usage, billions of gal/yr	25
Commercial, percent	80
Military, percent	20
Airforce	16
Navy	4
Fuel savings per year, millions of dollars	250
(Assumption: fuel cost of \$1/gal = 1 percent savings)	
Operational costs, percent	
Fighter aircraft	
Operations and support	45
Fuel	55
Commercial b747	
Operations and support	88
Fuel	22
Supersonic transport ^b	
Operations and support	70
Fuel	30

^aBased on information from M. Stibich and E.R. Mayhew, 1994,
WL/POTF, Wright Patterson Air Force Base, Dayton, Ohio.

^bEstimated from Uchida and Mizuno (1994).

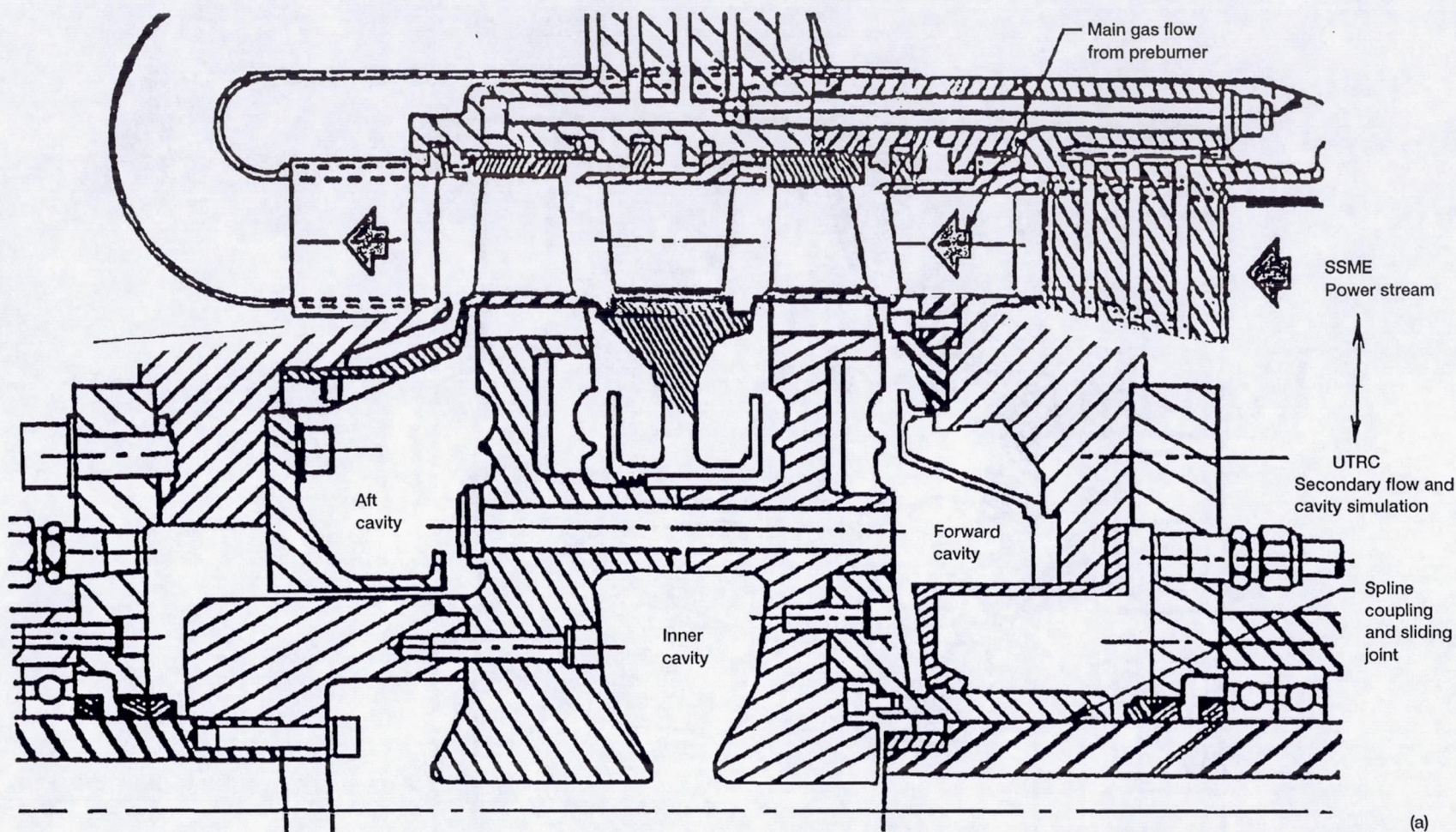


Figure 1.—Experimental apparatus simulating SSME high-pressure fuel turbopump (HPFTP) configuration (from Daniels and Johnson, 1993). Flow conditions: 1502 rpm; inlet axial velocity, 400 m/s; tangential velocity, 70 m/s; dimensionless purge flow parameters η_t of 0.002, 0.005, and 0.010. (a) Split view of SSME HPFTP and experimental cavities. (b) Flow regions. (c) Grid of composite geometry (right half of fig. 1(b)); body-fitted coordinates, 33 domains.

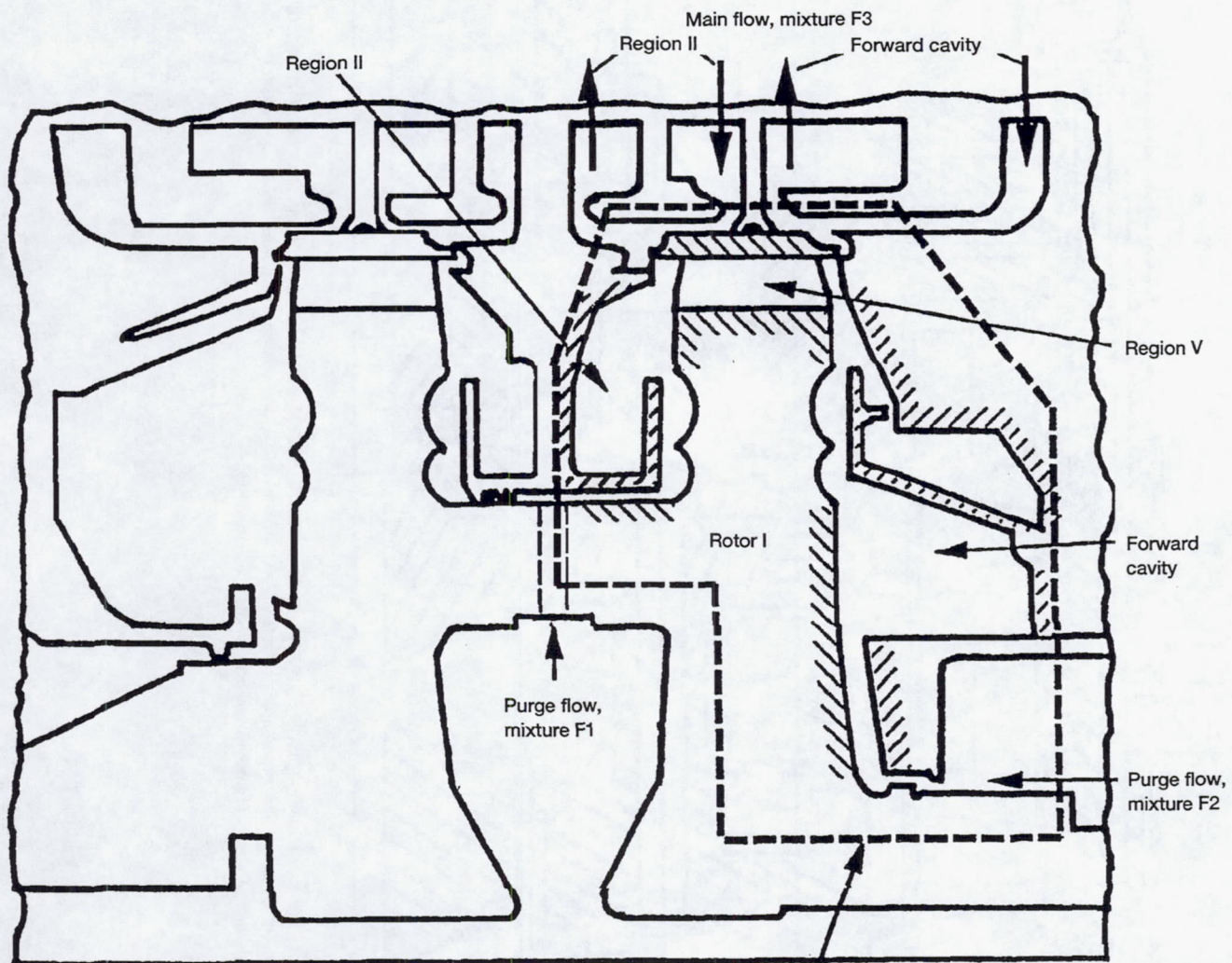


Figure 1.—Continued. (b) Flow regions.

(b)

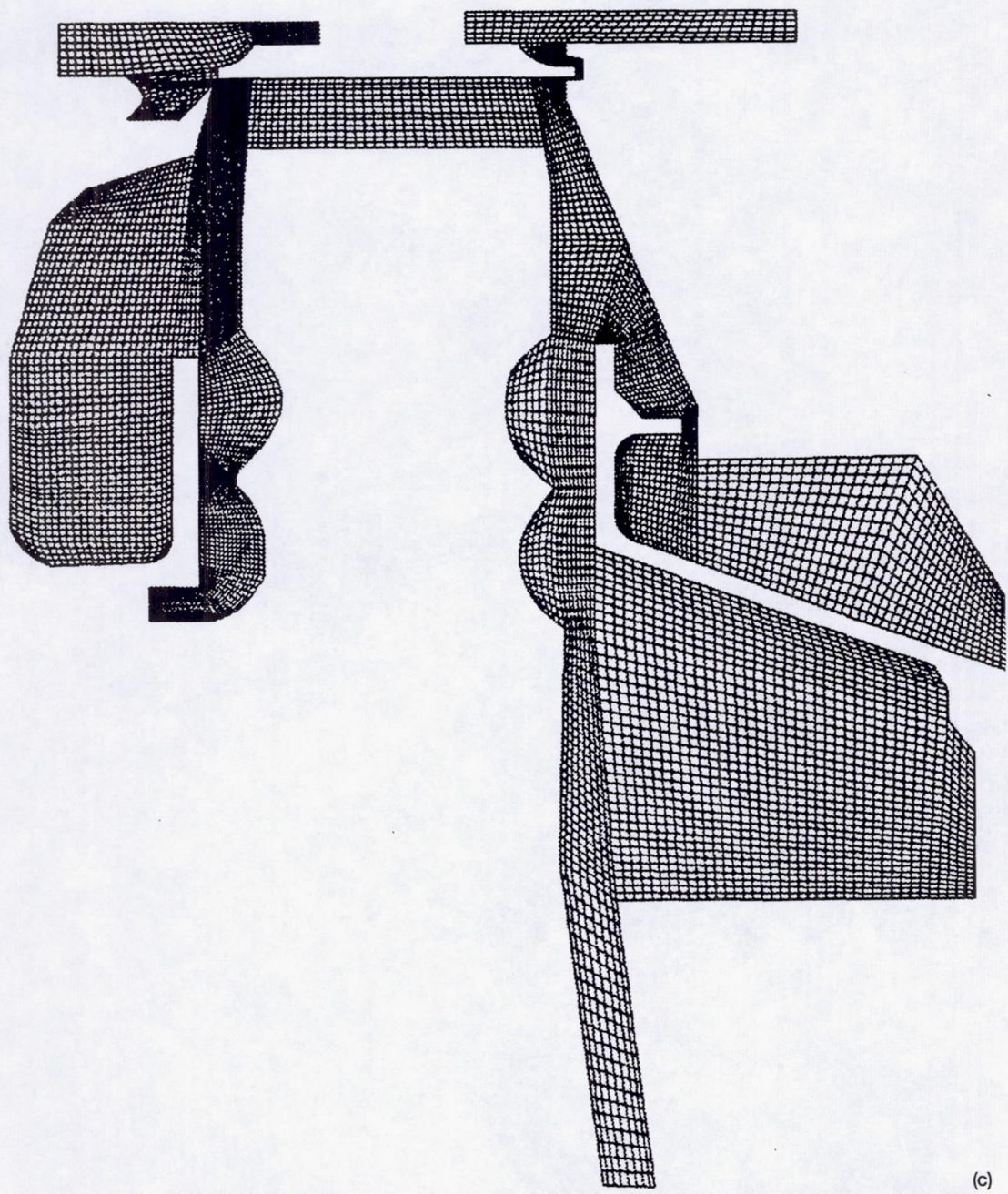


Figure 1.—Concluded. (c) Grid of composite geometry (right half of fig. 1(b)); body-fitted coordinates, 33 domains.

Page intentionally left blank

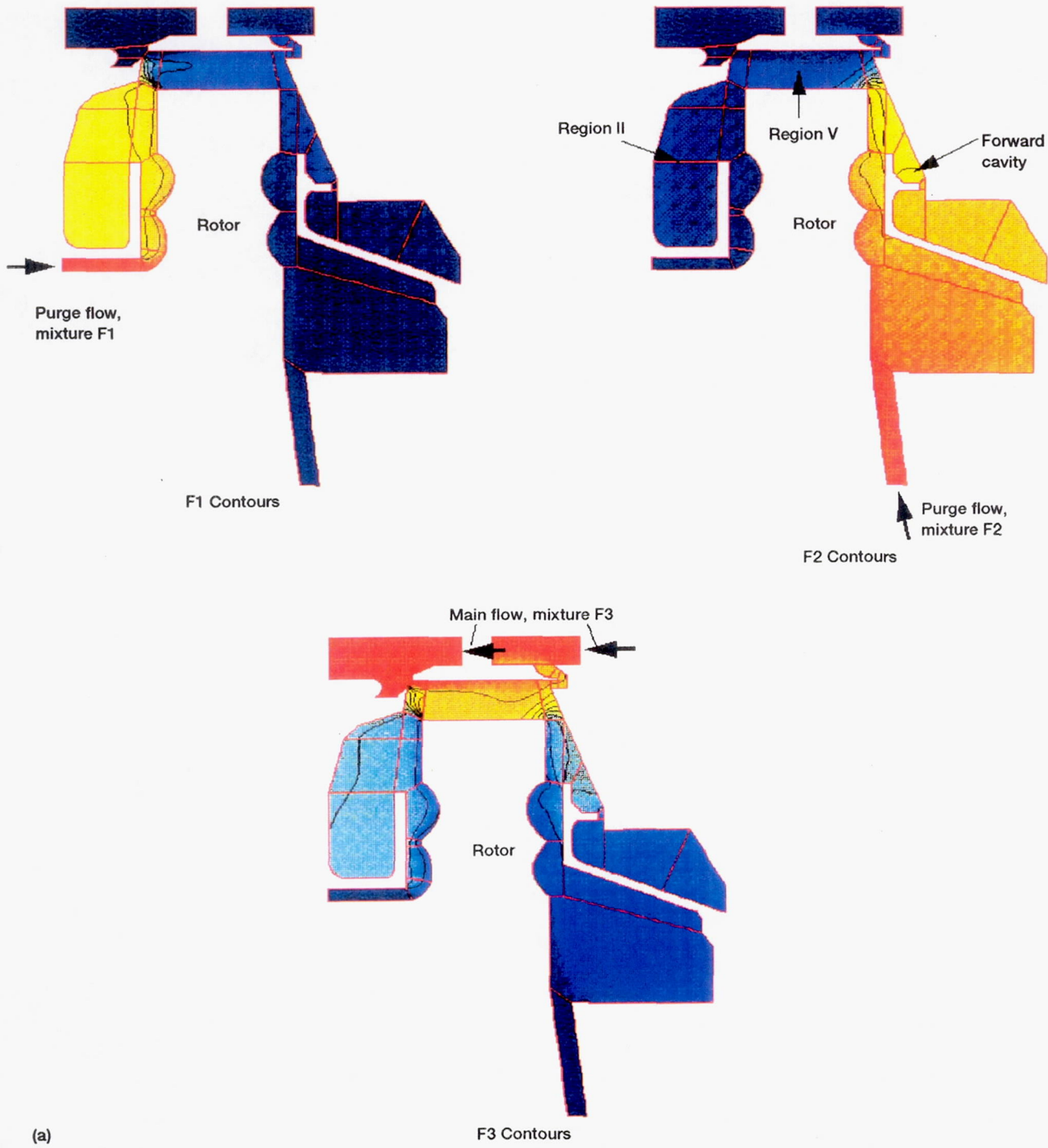


Figure 2.—Mixture fraction contours for purge sources F1, F2, and F3 for combined solutions of forward cavity, region II, and region V. Based on experiments of Daniels and Johnson (1993) for SSME HPFTP simulated configuration (right-hand portion of fig. 1 (a) or (b) with grid shown in fig. 1 (c)). (a) Dimensionless purge flow parameter, η_{lt} , 0.005. (b) Dimensionless purge flow parameter, η_{lt} , 0.010. (c) Dimensionless purge flow parameter, η_{lt} , 0.025.

Page intentionally left blank

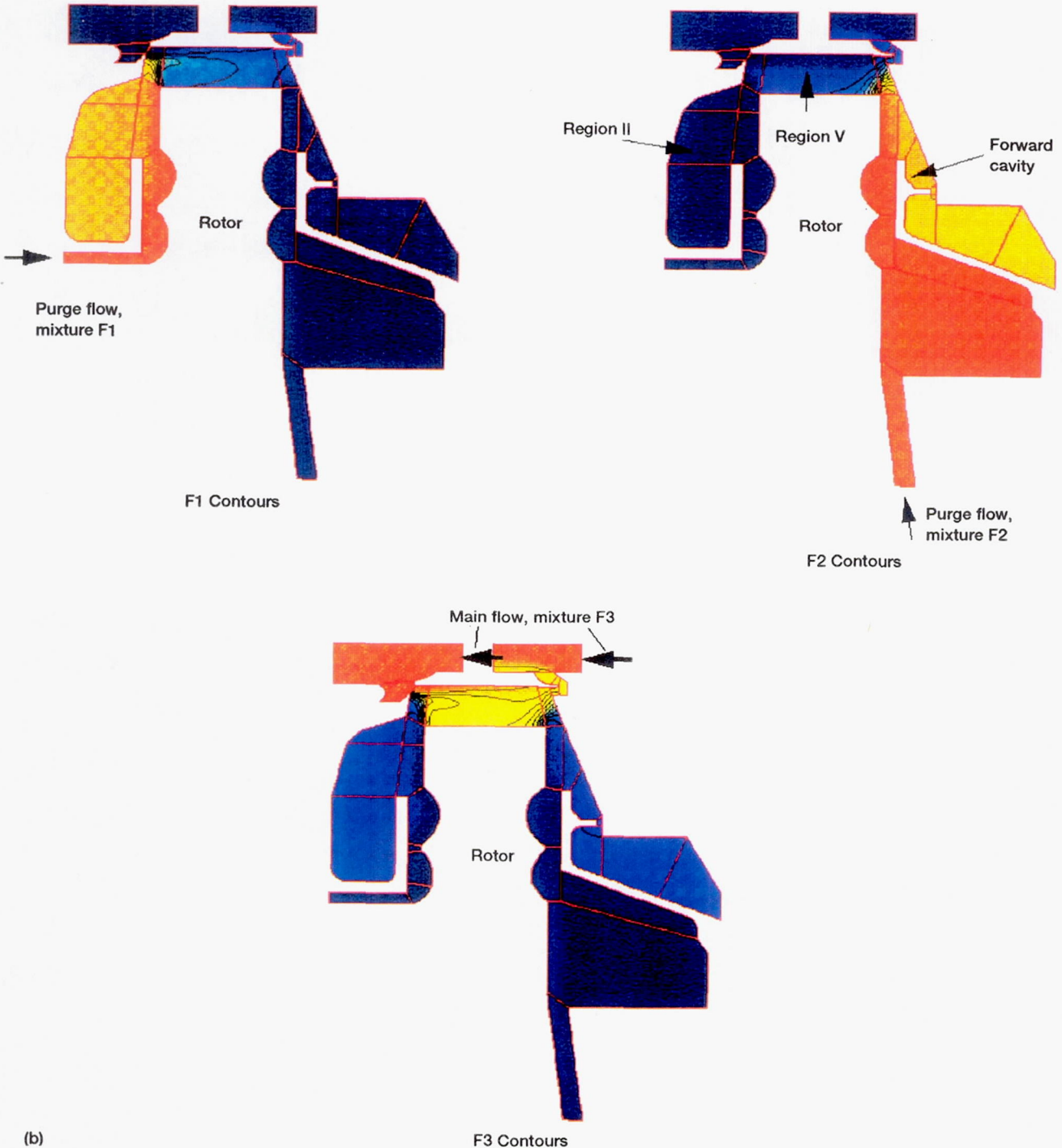


Figure 2.—Continued. (b) Dimensionless purge flow parameter, η_t , 0.010.

Page intentionally left blank

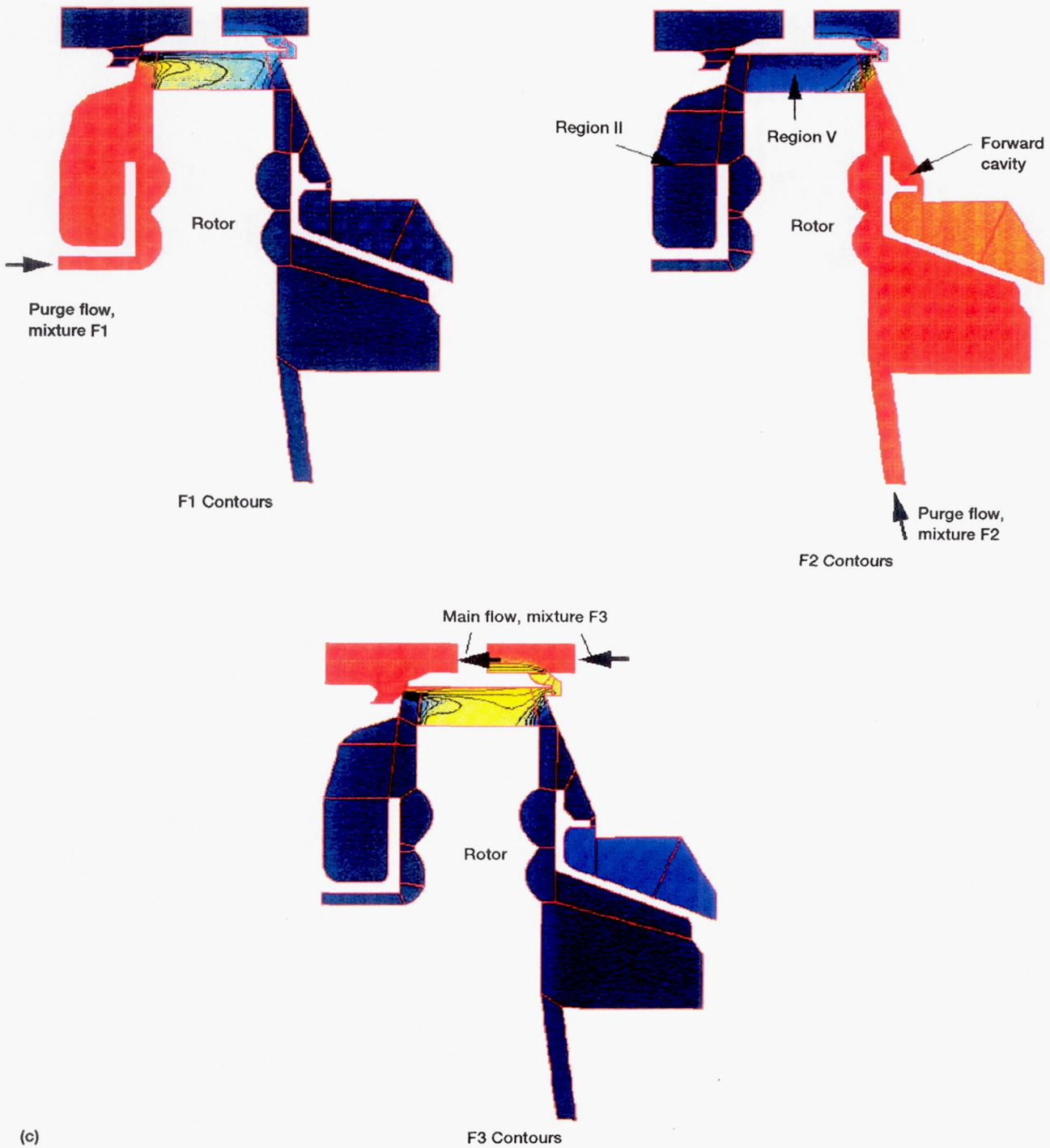


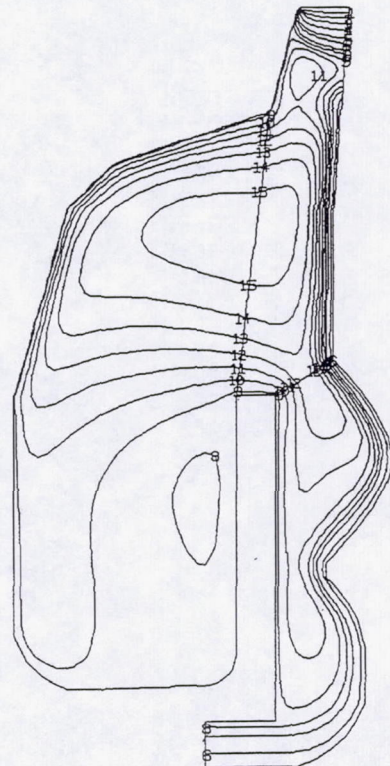
Figure 2.—Concluded. (c) Dimensionless purge flow parameter, η_{lb} , 0.025.

Page intentionally left blank

```

STRM  CONTOURS
FMIN  1.347E-07
FMAX  1.625E-02
CONTOUR LEVELS
 1  2.000E-03
 2  4.000E-03
 3  6.000E-03
 4  8.000E-03
 5  1.000E-02
 6  1.100E-02
 7  1.200E-02
 8  1.250E-02
 9  1.300E-02
10  1.350E-02
11  1.400E-02
12  1.450E-02
13  1.500E-02
14  1.550E-02
15  1.600E-02
OK>

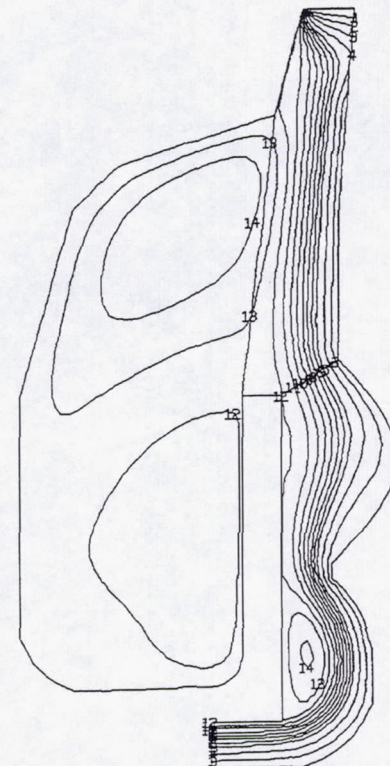
```



```

STRM  CONTOURS
FMIN  8.991E-08
FMAX  1.995E-02
CONTOUR LEVELS
 1  2.000E-03
 2  4.000E-03
 3  6.000E-03
 4  8.000E-03
 5  1.000E-02
 6  1.100E-02
 7  1.200E-02
 8  1.300E-02
 9  1.400E-02
10  1.500E-02
11  1.600E-02
12  1.700E-02
13  1.800E-02
14  1.900E-02
OK>

```



(a)

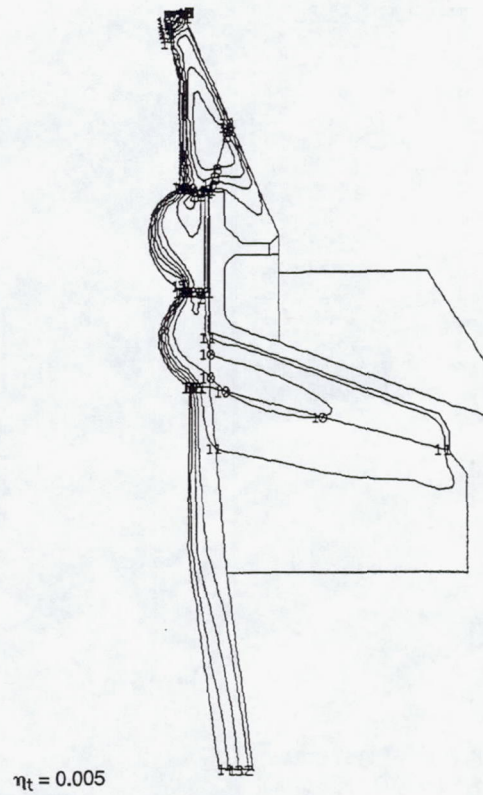
$\eta_t = 0.025$

Figure 3.—Flow streamlines for combined solutions of forward cavity, region II, and region V. Boundary conditions taken from experiments of Daniels and Johnson (1993) for SSME HPFTP simulated configuration for two dimensionless purge flow parameters η_t of 0.005 and 0.025. (a) Streamlines in flow region II. (b) Streamlines in forward cavity. (c) Power stream, rim seal, and region V. (d) Enlargement of upstream rim seal streamlines. (e) Enlargement of downstream rim seal streamlines. (f) Streamlines in main flow and seal regions. (g) Enlargement of downstream rim seal streamlines. (h) Ingestion of main-path flow in multiple-gas-turbine disk cavities.

```

STRM  CONTOURS
FMIN  1.565E-06
FMAX  1.407E-02
CONTOUR LEVELS
 2    7.420E-04
 4    2.223E-03
 6    3.704E-03
 8    5.184E-03
10    6.665E-03
12    8.146E-03
14    9.627E-03
16    1.111E-02
18    1.259E-02
20    1.407E-02
OK>

```



```

STRM  CONTOURS
FMIN -1.856E-02
FMAX  5.210E-03
CONTOUR LEVELS
 1    -1.856E-02
 2    -1.686E-02
 3    -1.517E-02
 4    -1.347E-02
 5    -1.177E-02
 6    -1.007E-02
 7    -8.374E-03
 8    -6.676E-03
 9    -4.978E-03
10    -3.280E-03
11    -1.582E-03
12    1.159E-04
13    1.814E-03
14    3.512E-03
15    5.210E-03
OK>

```

(b)

$\eta_t = 0.025$

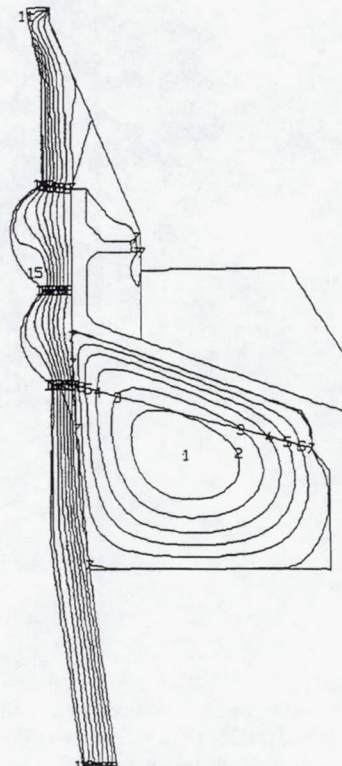
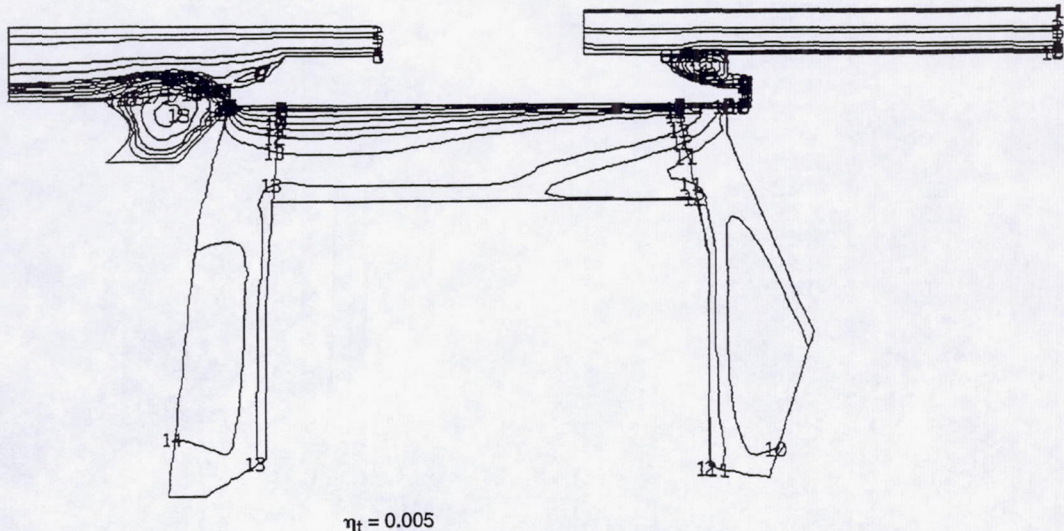


Figure 3.—Continued. (b) Streamlines in forward cavity.

```

STRM  CONTOURS
FMIN -1.044E-01
FMAX 3.172E-02
CONTOUR LEVELS
 1 -1.000E-01
 2 -6.000E-02
 3 -2.000E-02
 4 -1.000E-02
 5 -5.000E-02
 6 -1.000E-03
 7 1.000E-03
 8 2.000E-03
 9 4.000E-03
10 6.000E-03
11 8.000E-03
12 1.000E-02
13 1.250E-02
14 1.500E-02
15 1.750E-02
16 2.000E-02
17 2.500E-02
18 3.000E-02
OK>

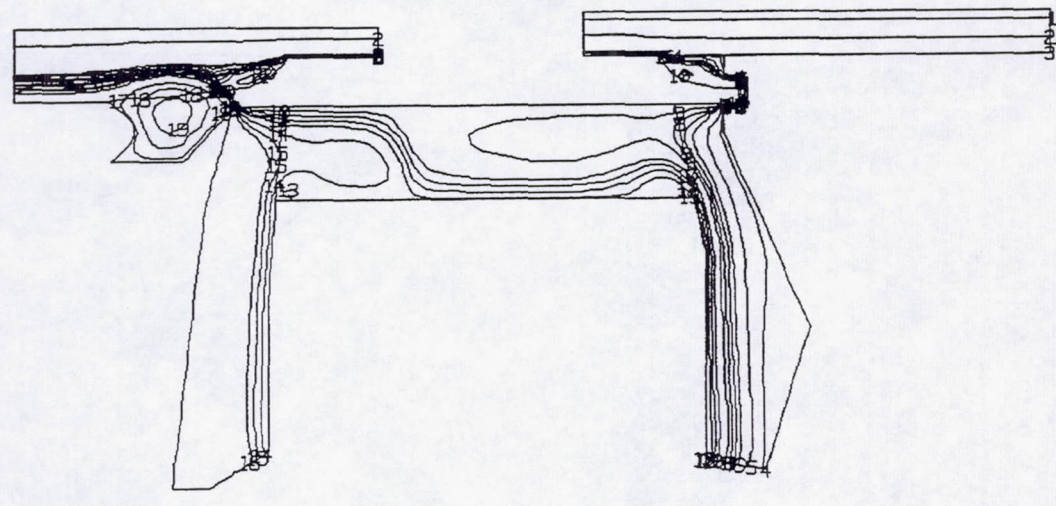
```



```

STRM  CONTOURS
FMIN -1.204E-01
FMAX 4.555E-02
CONTOUR LEVELS
 1 -1.000E-01
 2 -5.000E-02
 3 -1.000E-02
 4 -8.000E-03
 5 -6.000E-03
 6 -4.000E-03
 7 -3.000E-03
 8 -2.000E-03
 9 -1.000E-03
10 1.000E-03
11 2.000E-03
12 3.000E-03
13 4.000E-03
14 6.000E-03
15 8.000E-03
16 1.000E-02
17 2.000E-02
18 3.000E-02
19 4.000E-02
OK>

```



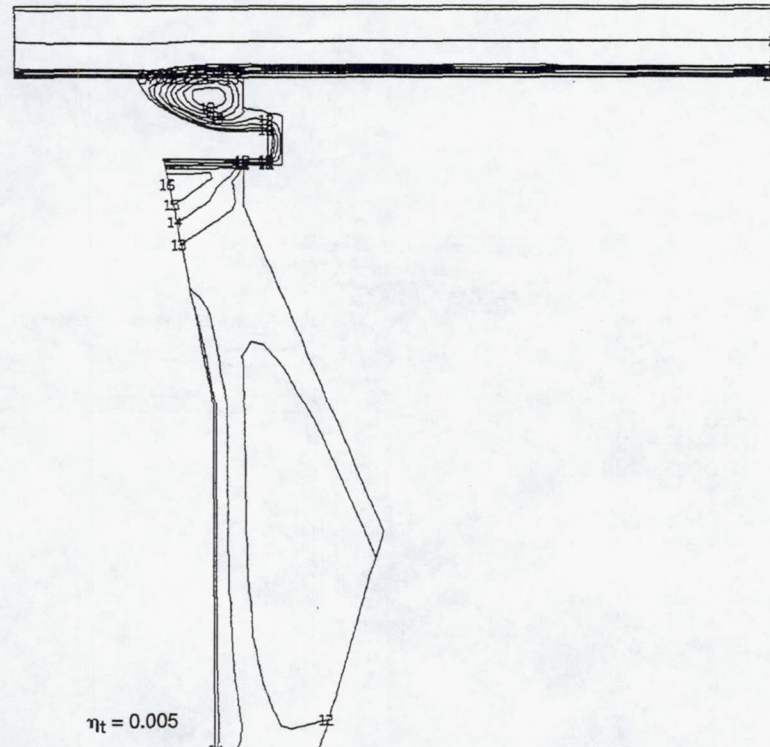
(c)

Figure 3.—Continued. (c) Power stream, rim seal, and region V.

```

STRM  CONTOURS
FMIN -1.044E-01
FMAX  1.576E-02
CONTOUR LEVELS
 1  -1.000E-01
 2  -5.000E-02
 3  -1.000E-02
 4  -8.000E-03
 5  -6.000E-03
 6  -4.000E-03
 7  -2.000E-03
 8  -1.000E-03
 9   1.000E-03
10   2.000E-03
11   4.000E-03
12   6.000E-03
13   8.000E-03
14   1.000E-02
15   1.200E-02
16   1.400E-02
OK>

```

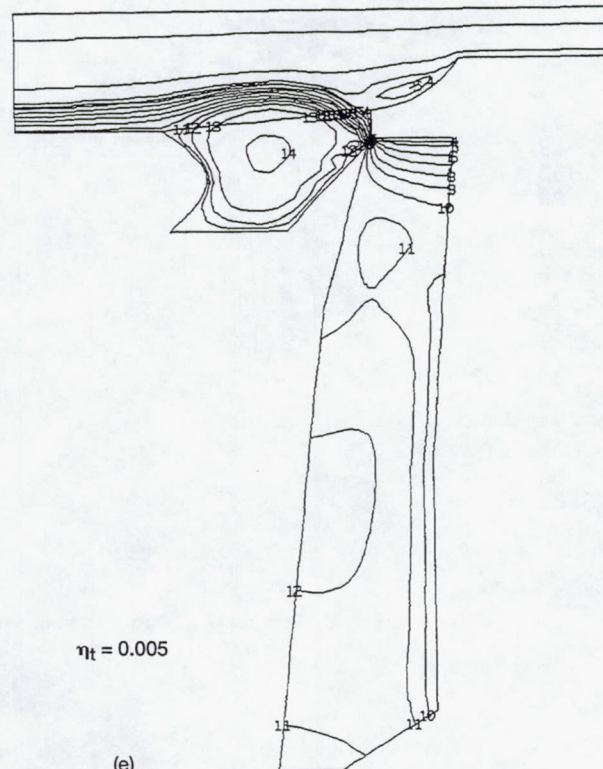


(d)

```

STRM  CONTOURS
FMIN -7.391E-02
FMAX  3.172E-02
CONTOUR LEVELS
 1  -5.000E-02
 2  -1.000E-02
 3  -1.000E-03
 4   1.000E-03
 5   2.000E-03
 6   4.000E-03
 7   6.000E-03
 8   8.000E-03
 9   1.000E-02
10   1.200E-02
11   1.400E-02
12   1.600E-02
13   2.000E-02
14   3.000E-02
OK>

```



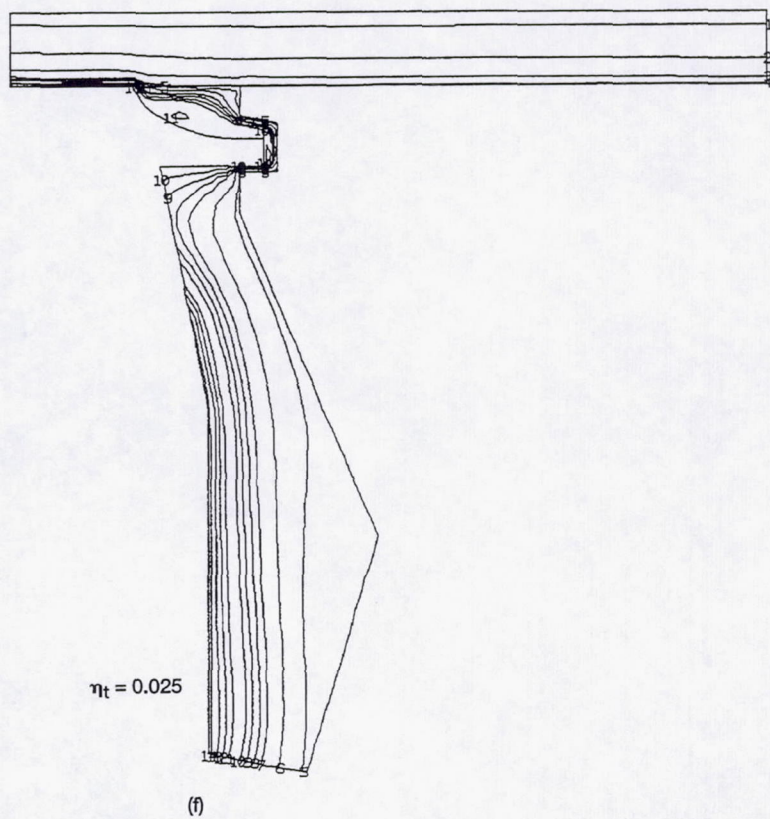
(e)

Figure 3.—Continued. (d) Enlargement of upstream rim seal streamlines. (e) Enlargement of downstream rim seal streamlines.

```

STRM  CONTOURS
FMIN -1.204E-01
FMAX 4.247E-03
CONTOUR LEVELS
 1  -1.000E-01
 2  -5.000E-02
 3  -2.000E-02
 4  -1.000E-02
 5  -8.000E-03
 6  -6.000E-03
 7  -4.000E-03
 8  -3.000E-03
 9  -2.000E-03
10  -1.000E-03
11  1.000E-03
12  2.000E-03
13  3.000E-03
14  4.000E-03
OK>

```



```

STRM  CONTOURS
FMIN -7.391E-02
FMAX 4.555E-02
CONTOUR LEVELS
 1  -5.000E-02
 2  -1.000E-02
 3  -1.000E-03
 4  1.000E-03
 5  2.000E-03
 6  4.000E-03
 7  6.000E-03
 8  8.000E-03
 9  1.000E-02
10  2.000E-02
11  3.000E-02
12  4.000E-02
OK>

```

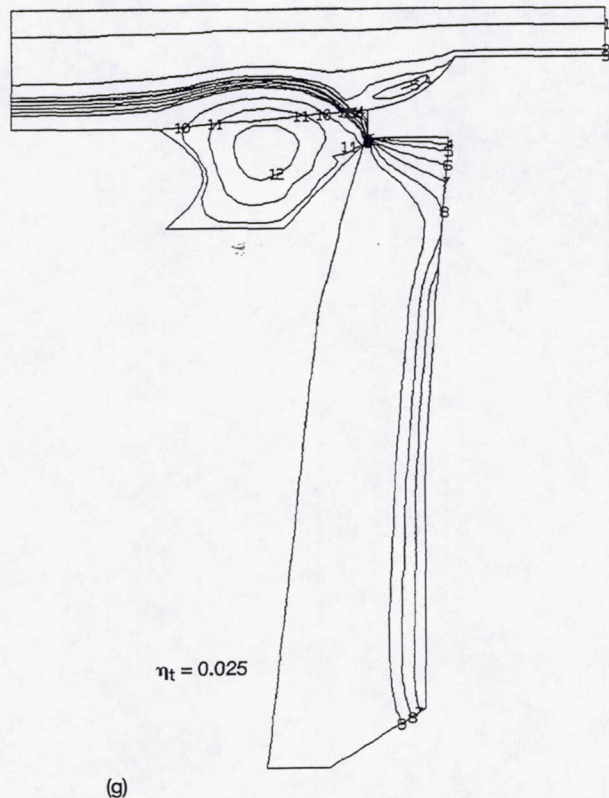
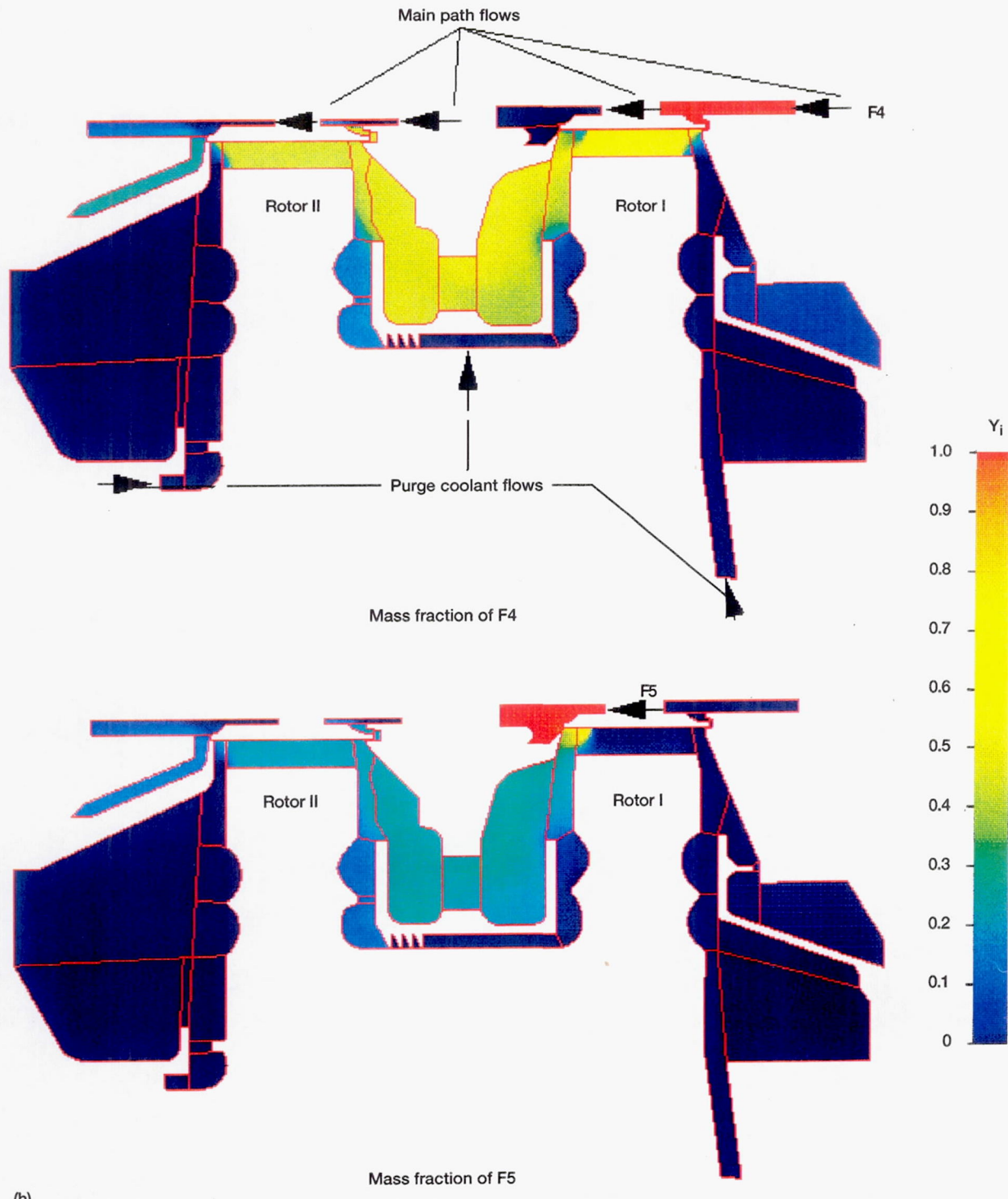


Figure 3.—Concluded. (f) Streamlines in main flow and seal regions. (g) Enlargement of downstream rim seal streamlines.

Page intentionally left blank



(h)

Figure 3.—Concluded. (h) Ingestion of main-path flow in multiple-gas-turbine disk cavities.

Page intentionally left blank

```

XY PLANE 1
F1    CONTOURS
FMIN 0.000E+00
FMAX 1.000E+00
CONTOUR LEVELS
 1 0.000E+00
 2 1.000E-01
 3 2.000E-01
 4 3.000E-01
 5 4.000E-01
 6 5.000E-01
 7 6.000E-01
 8 7.000E-01
 9 8.000E-01
10 9.000E-01
11 1.000E+00
OK>

```

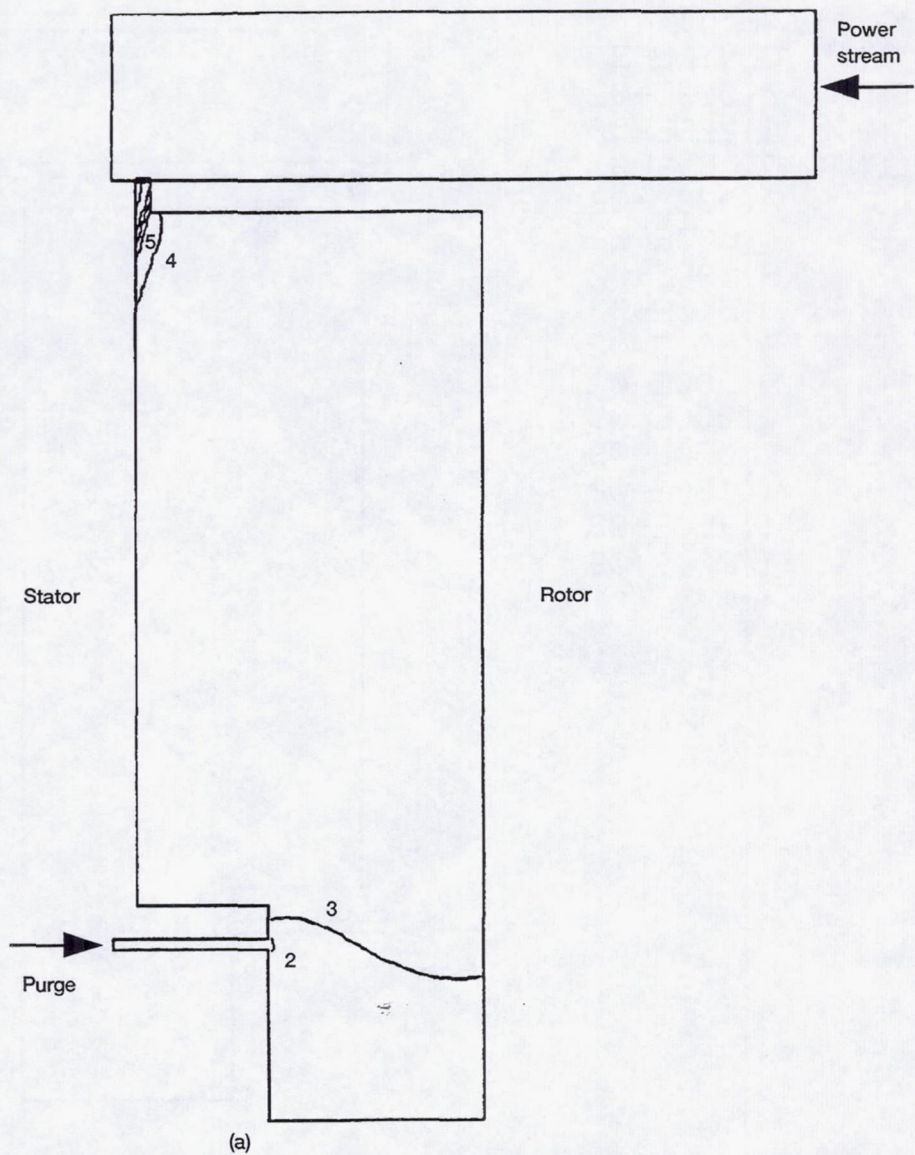


Figure 4.—Comparison of CO_2 dilution and temperature contours for dimensionless purge flow parameters η_t of 0.001 and 0.008. UTRC cavity configuration 1 (Graber et al., 1987); inlet pressure, 860 kPa; inlet temperature, 1200 K; purge flow pressure, 690 kPa; purge flow temperature, 700 K; axial velocity, 400 m/s; inlet swirl at rotor tip speed. (a) CO_2 contours; $\eta_t = 0.001$. (b) Temperature contours; $\eta_t = 0.001$. (c) CO_2 contours; $\eta_t = 0.008$. (d) Temperature contours; $\eta_t = 0.008$.

XY PLANE 1
 TEMP CONTOURS
 FMIN 7.003E+02
 FMAX 1.226E+03
 CONTOUR LEVELS
 1 7.000E+02
 2 7.500E+02
 3 8.000E+02
 4 8.500E+02
 5 9.000E+02
 6 9.500E+02
 7 1.000E+03
 8 1.050E+03
 9 1.100E+03
 10 1.150E+03
 11 1.200E+03
 OK>

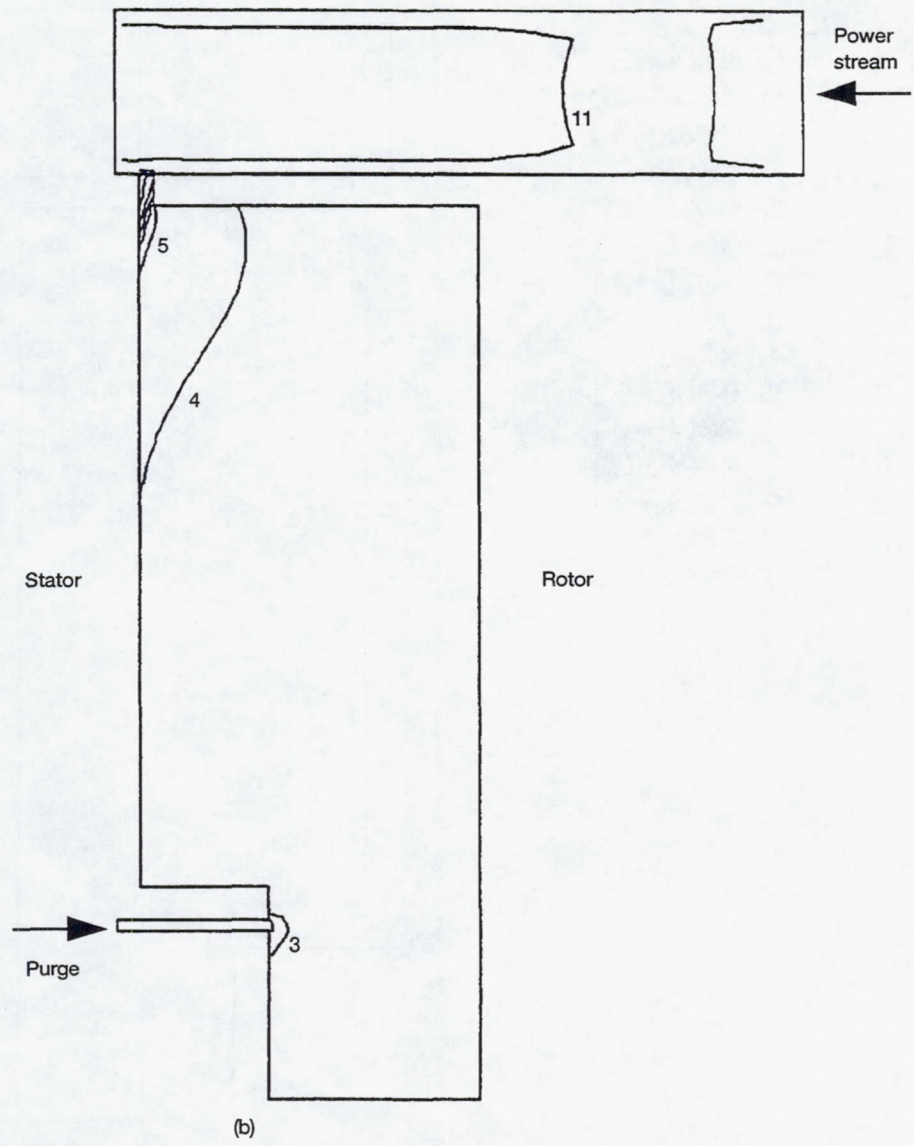


Figure 4.—Continued. (b) Temperature contours; $\eta_t = 0.001$.

```

XY PLANE 1
F1    CONTOURS
FMIN  0.000E+00
FMAX  1.000E+00
CONTOUR LEVELS
 1  0.000E+00
 2  1.000E-01
 3  2.000E-01
 4  3.000E-01
 5  4.000E-01
 6  5.000E-01
 7  6.000E-01
 8  7.000E-01
 9  8.000E-01
10  9.000E-01
11  1.000E+00
OK>

```

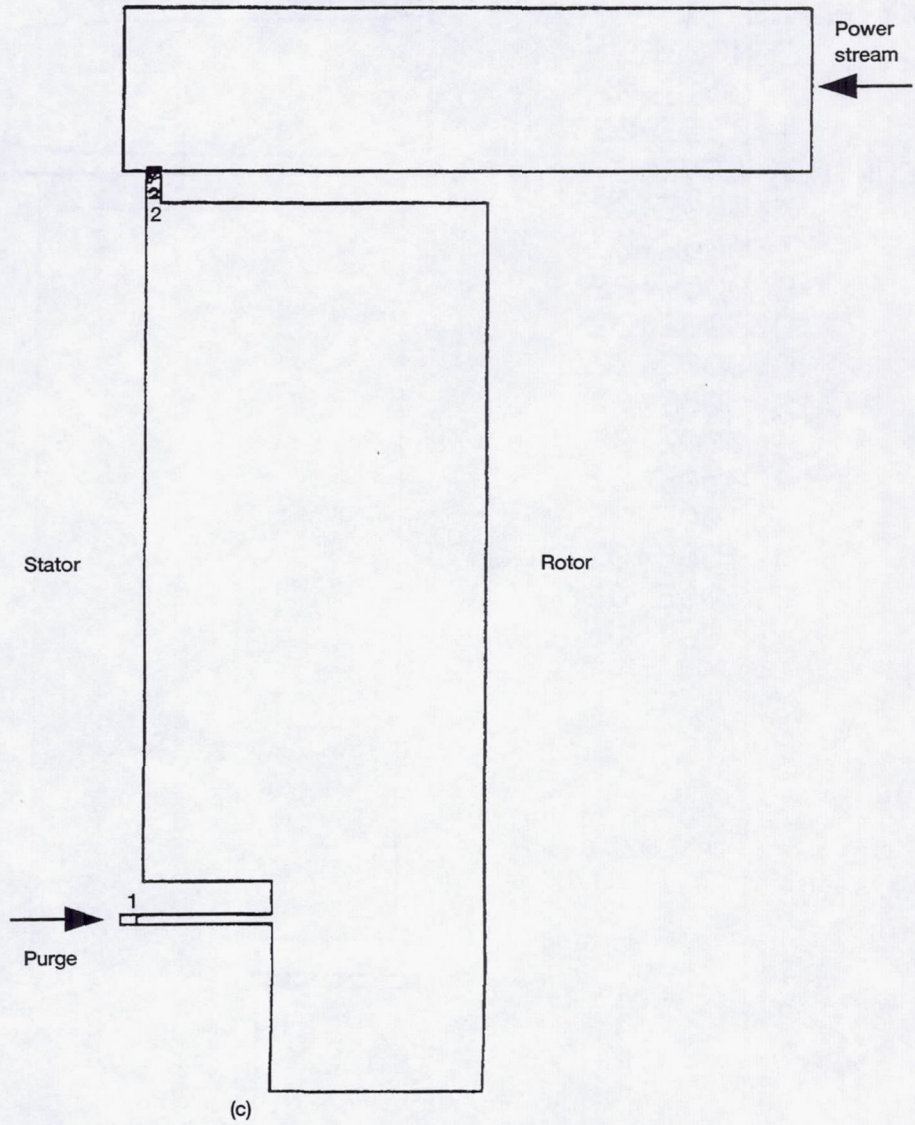


Figure 4.—Continued. (c) CO_2 contours; $\eta_t = 0.008$.

XY PLANE 1
 CONTOURS
 7.001E+02
 1.225E+03
 CONTOUR LEVELS
 7.000E+02
 7.500E+02
 8.000E+02
 8.500E+02
 9.000E+02
 9.500E+02
 1.000E+03
 1.050E+03
 1.100E+03
 1.150E+03
 1.200E+03

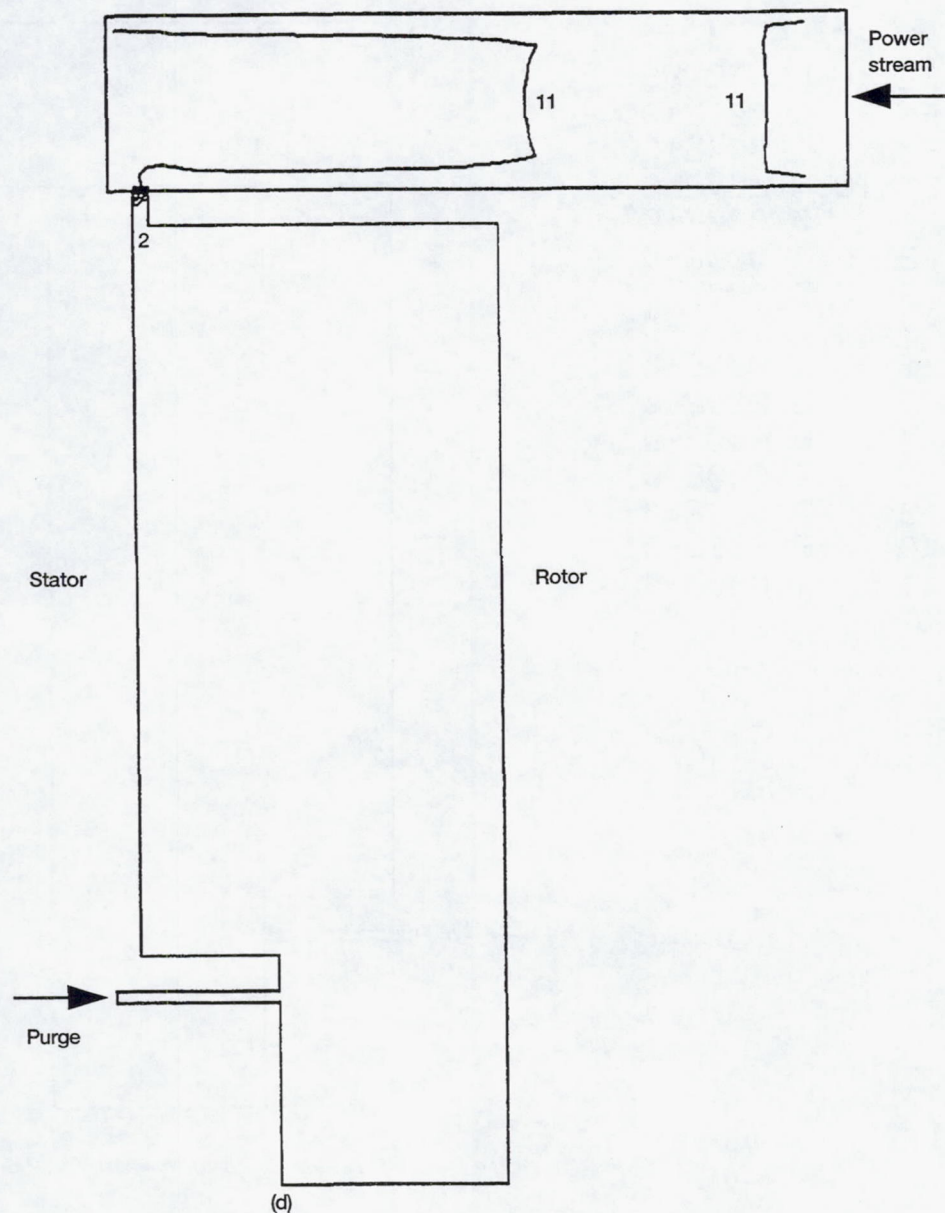


Figure 4.—Concluded. (d) Temperature contours; $\eta_{lt} = 0.008$.

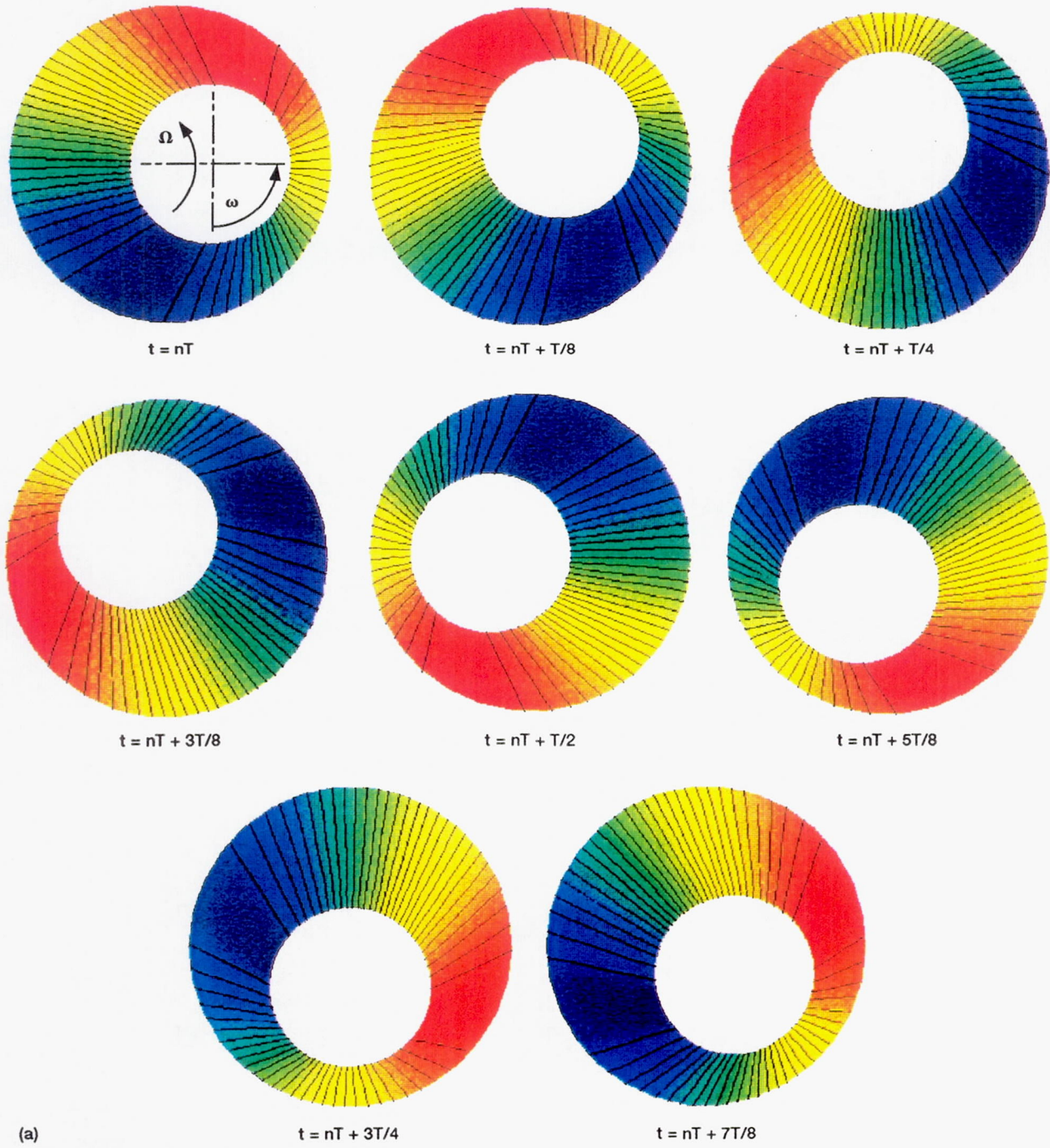


Figure 5.—Time-dependent solutions of perturbation pressure. Plane of view at half seal length. Eccentricity ϵ normalized by clearance c_o , where e_s is static and e_d is dynamic eccentricity; ω is shaft angular rotational speed, and Ω is whirl speed.
 (a) $\epsilon_s = e_s/c_o = 0.0$; $\epsilon_d < 0.001$ $\epsilon = e_d/c_o$; $\Omega = 2.0 \omega$. (b) $\epsilon_s = e_s/c_o = 0.7$; $\epsilon_d < 0.001$ $\epsilon = e_d/c_o$; $\Omega = 2.5 \omega$.

Page intentionally left blank

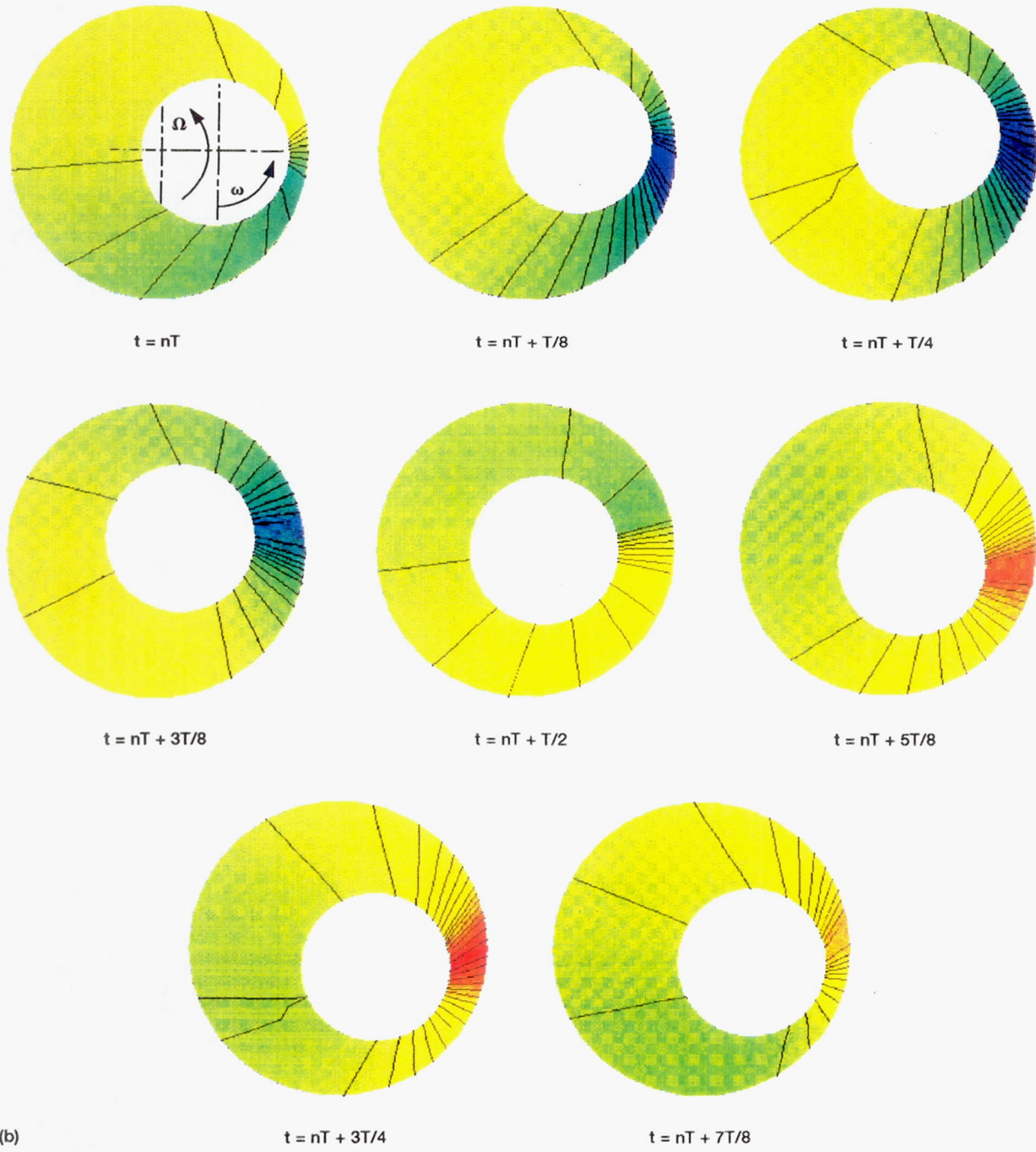


Figure 5.—Concluded. (b) $\epsilon_s = e_s/c_o = 0.7$; $\epsilon_d < 0.001$ $\epsilon = e_d/c_o$; $\Omega = 2.5 \omega$.

REPORT DOCUMENTATION PAGE

*Form Approved
OMB No. 0704-0188*

Public reporting burden for this collection of information is estimated to average 1 hour per response, including the time for reviewing instructions, searching existing data sources, gathering and maintaining the data needed, and completing and reviewing the collection of information. Send comments regarding this burden estimate or any other aspect of this collection of information, including suggestions for reducing this burden, to Washington Headquarters Services, Directorate for Information Operations and Reports, 1215 Jefferson Davis Highway, Suite 1204, Arlington, VA 22202-4302, and to the Office of Management and Budget, Paperwork Reduction Project (0704-0188), Washington, DC 20503.

1. AGENCY USE ONLY (Leave blank)			2. REPORT DATE May 1995		3. REPORT TYPE AND DATES COVERED Technical Memorandum		
4. TITLE AND SUBTITLE Comparison of Numerical Results and Multicavity Purge and Rim Seal Data With Extensions to Dynamics			5. FUNDING NUMBERS WU-232-01-02				
6. AUTHOR(S) Mahesh M. Athavale, Andrzej J. Przekwas, Robert C. Hendricks, and Bruce M. Steinetz							
7. PERFORMING ORGANIZATION NAME(S) AND ADDRESS(ES) National Aeronautics and Space Administration Lewis Research Center Cleveland, Ohio 44135-3191			8. PERFORMING ORGANIZATION REPORT NUMBER E-9039				
9. SPONSORING/MONITORING AGENCY NAME(S) AND ADDRESS(ES) National Aeronautics and Space Administration Washington, D.C. 20546-0001			10. SPONSORING/MONITORING AGENCY REPORT NUMBER NASA TM-106685				
11. SUPPLEMENTARY NOTES Prepared for the Third Northern Ohio Technical Symposium "Aerospace Today" sponsored by the American Institute of Aeronautics and Astronautics, Cleveland, Ohio, May 16, 1994. Mahesh M. Athavale and Andrzej J. Przekwas, CFD Research Inc., Huntsville, Alabama 35805; Robert C. Hendricks and Bruce M. Steinetz, NASA Lewis Research Center. Responsible person, R.C. Hendricks, organization code 5300, (216) 433-7507.							
12a. DISTRIBUTION/AVAILABILITY STATEMENT Unclassified - Unlimited Subject Categories 20 and 22			12b. DISTRIBUTION CODE				
13. ABSTRACT (Maximum 200 words) The computation of flows within interconnected, multiple-disk cavities shows strong interaction between the cavities and the power stream. For this reason, simulations of single cavities in such cases are not realistic; the complete, linked configuration must be considered. Unsteady flow fields affect engine stability and can engender power-stream-driven secondary flows that produce local hot spotting or general cavity heating. Further, a concentric whirling rotor produces a circumferential pressure wave, but a statically eccentric whirling rotor produces a radial wave; both waves affect cavity ingestion and the stability of the entire engine. It is strongly suggested that seals be used to enhance turbojet engine stability. Simple devices, such as swirl brakes, honeycomb inserts, and new seal configurations, should be considered. The cost effectiveness of the NASA Lewis Research Center seals program can be expressed in terms of program goals (e.g., the Integrated High-Pressure/Temperature Engine Technology (IHPTET) cannot be achieved without such a program), cost (savings to \$250 million/1-percent decrease in specific fuel consumption), and indirect benefits (reduction of atmospheric NO _x and CO ₂ and reduction of powerplant downtime).							
14. SUBJECT TERMS Seals; Cavities; Flow ingestion; Dynamics				15. NUMBER OF PAGES 26			
				16. PRICE CODE A03			
17. SECURITY CLASSIFICATION OF REPORT Unclassified		18. SECURITY CLASSIFICATION OF THIS PAGE Unclassified		19. SECURITY CLASSIFICATION OF ABSTRACT Unclassified		20. LIMITATION OF ABSTRACT	